Published by IOP Publishing for Sissa Medialab

Received: *February 6, 2025*
Accepted: *February 19, 2025*
Published: *March 27, 2025*

The 15th International Symposium on Electron Beam Ion Sources and Traps
Kielce, Poland
27–30 August 2024

Attaining high charge states with REXEBIS

A. Gunnarsson,[a,d] **N. Bidault**[b] **C. Munoz Diaz**[c] **H. Pahl**[d] **A. Pikin**[d,e] **and F. Wenander**[d,*]

[a] *Department of Physics, University of Gothenburg, Gothenburg, S-412 96, Sweden*
[b] *Department of Physics and Astronomy, University of Hawaii Manoa, HI 96822, Honolulu, U.S.A.*
[c] *Institute of Particle Physics and Accelerator Technologies at Riga Technical Unversity, 1048 Riga, Latvia*
[d] *European Organization for Nuclear Research, Esplanade des Particules 1, 1211 Geneva 23, Switzerland*
[e] *Centro de Investigaciones Energeticas, Medioambientales y Technologicas, Avendia Complutense 40, 28040 Madrid, Spain*

E-mail: fredrik.wenander@cern.ch

Abstract: At REXEBIS, a higher electron current density accelerates charge breeding and allows for increased repetition rate and ion throughput of the REX-ISOLDE system, while also extending the physics reach towards very short-lived radioactive ions. This goal was pursued by introducing a non-adiabatic electron gun. Since then, further breeding characterization experiments have been carried out, focusing on reaching very high charge states for light ions, such that a closed-shell configuration with exceptionally high breeding efficiency is attained, and to lower the mass-to-charge ratio for heavy elements thereby alleviating the required acceleration gradient in the room-temperature section of the LINAC. The results are discussed and extensively compared with predictions from the *ebisim* charge breeding simulation code. In order to explain discrepancies in the charge breeding efficiency and an apparent excessive electron current density for heavy elements, the effect of applying different electron-ion impact ionisation models was investigated, as well as contributions from collisional excitation followed by auto-ionisation.

Keywords: Ion sources (positive ions, negative ions, electron cyclotron resonance (ECR), electron beam (EBIS)); Ionization and excitation processes

*Corresponding author.

https://doi.org/10.1088/1748-0221/20/03/C03053

2025 JINST 20 C03053

Contents

1 Introduction

REXEBIS, the EBIS-based charge breeder for HIE-ISOLDE, was originally designed to provide beams of moderate mass-to-charge (A/Q) ratios, with an upper limit of A/Q = 4.5 imposed by the RF cavities of the fixed-velocity room-temperature section of the post-accelerating LINAC [1]. With the later addition of individually tuned superconducting quarter-wave cavities [2], downstream of the room-temperature section, higher charge states have become of interest as they allow for an increased final beam energy according to eq. (1.1).

$$W_{\text{final}} = 2.85 + \frac{Q}{A} \cdot U_{\text{acc}} \qquad \left[\text{MeV u}^{-1}\right] \tag{1.1}$$

For instance, with ions of A/Q=3, a beam energy of 12.8 MeV u^{-1} should in principle be attainable for the design acceleration voltage of 30 MV in the superconducting part. Such high energies have not been reached due to a gradual degradation of the accelerating field in the cavities, which presently limits the operational voltage to 19.2 MV (as of 2023). A further motivation for higher charge states delivered by the EBIS originates from undesirable instabilities in the RF-system for the room-temperature section of the LINAC at higher power levels. Thus today ions must have a A/Q≤4 for operation stability, creating challenges for the charge breeding system in particular for very heavy beams (A>180). The original electron gun, with a limited operational electron current density of approximately 100 A cm^{-2} [3], could not fulfill these requirements. Moreover, creating few-electron configurations, such as K^{17+}, resulted in long charge breeding times and poor single charge state efficiency, and for the heaviest transported element, i.e. uranium, the charge state distribution did not peak at the selected 54+ charge state even for charge breeding times exceeding 500 ms, most likely due to neutralisation of the space-charge potential allowing ions to escape from the electron beam potential well.

In 2020 a new gun was installed and commissioned at REXEBIS. The gun is still of immersed magnetic-field type, however, a non-adiabatic magnetic field modulation was introduced in the gun region to allow for a reduced cathode flux and greater electron beam compression in the magnetic field [4]. A thorough evaluation of the gun was performed at the commissioning stage, with the results presented in ref. [5]. With the recent requests for higher charge states in mind, another

2025 JINST 20 C03053

measurement campaign was carried out, where the charge state limits and the effective electron current density were put in focus. For example, we have previously observed a variation in the estimated electron current density derived from charge breeding tests of different elements. As seen in ref. [5], heavier and more highly charged elements yield a higher estimate for the current density than lighter elements. Ion heating effects and non-negligible 1+ ion injection energy, causing elements to only partially be superimposed by the ionising electron beam (i.e. the overlap factor $f_{ei} < 1$) can affect the effective current density. However, energy spread measurements of the ion populations did in general not support the idea of large radial excursions of the ions. Special attention was therefore paid to this anomaly during the measurement series. Likewise, we focused on the striking step in single charge-state efficiency (defined as the ratio of extracted n+ to injected 1+ ions), when going from K^{8+} to K^{9+}. The phenomenon has been consistently recorded at REXEBIS on different occasions, but is not reproduced in charge breeding simulations, where the change in efficiency is only minor. This has led us to believe that the modelling of the electron-ion impact ionisation (EI) cross-sections near closed-shell configurations (Ne-like) is incorrect, or that the simulation code does not replicate the ion injection conditions correctly.

In light of the high effective current density recorded for heavy elements, which has also been reported by other setups [6, 7], we have dedicated a section to investigate the differences in EI cross-sections obtained for high charge states of uranium by implementing various EI models. Additionally, studies of indirect ionisation processes have been carried out, through electron impact excitation and subsequent autoionisation, for ($Kr^{5+,6+,10+,15+,17+}$) [8], (Ti^{3+}, Zr^{3+}, Hf^{3+}) [9] and (C^{3+}, N^{4+}, O^{5+}) [10], with results showing significant contributions to the total ionisation cross-section for some ions. Intrigued by these results, we have performed simplified calculations to estimate the excitation-autoionisation cross-section for high charge states of uranium.

In these studies we have made extensive use of the *ebisim* charge breeding code [11] to evaluate the effects of different atomic physics phenomena, and to gauge the influence of possible neutralisation of the electron beam on the breeding process. It has been an opportunity to benchmark the core of the code under strict conditions, and to identify features to be implemented in future versions.

2 The EBISIM code

To aid with the interpretation of experimental data, and to understand better the contributions of various effects to the overall charge breeding dynamics, we employ computer simulations. In these studies, we mostly use the *ebisim* toolbox [11], a Python package which we have developed. A full description of the simulation package, including all mathematical modelling expressions, would go far beyond the scope of this document and the interested reader is referred to ref. [12] for an in-depth description. Here, a brief conceptual description of the *ebisim* modelling is provided.

The *ebisim* package uses the established technique of describing the charge breeding process with a set of coupled rate equations, which are integrated numerically from some initial value to predict the evolution of the ion density and temperature in given charge states as a function of time [13]. Exploiting the translational symmetry along the trap axis, which is typical for an EBIS, the rate equations are expressed in terms of the linear ion density (i.e. particles per unit length), the volumetric density is determined on demand as will be described below. Further, we have found an improvement in numerical stability by expressing the energy flow in terms of the ion temperature rates instead of tracking the energy density, as is common practice. It should be noted that *ebisim*, just as in other

2025 JINST 20 C03053

simulation codes, is built on the assumption that identical ions thermalise sufficiently quickly that they can be described as a thermal ensemble with a well-defined temperature at all times.

The single most important process to consider in an EBIS is EI. As a beam-driven process, the rate of ionisation scales with the electron current density j, the geometric overlap of the ion cloud and electron beam f_{ei}, and the associated cross-section σ_i^{EI}, which generally depends on the charge state i of the ion and the energy of the impinging electron E_e. In *ebisim* the cross-section for (single-step) EI is computed from a fully implemented Lotz model [14–17], paired with a catalogue of subshell binding energies for all elements [18]. Relativistic corrections [19, 20] are implemented but considered insignificant for the studies presented here.

EI is competing with beam-driven recombination processes, the most important being Radiative Recombination (RR), where a beam electron is captured by a highly charged ion. The rates for this process are expressed in close analogy to the modelling of EI, and we use the established empirical Kim & Pratt model [21] to compute the interaction cross-sections for RR. Dielectronic Recombination (DR) is a close but resonant cousin to RR and can generally be considered in *ebisim* if the required transition- and capture-strengths are provided (*ebisim* ships with tables for KLL-type transitions). In the context of this study, we consider DR irrelevant due to its narrow resonance lines, which are washed out by the electron beam's energy spread.

The ion charge state can also be reduced in collisions with neutral background atoms, where an electron is transferred from the neutral atom to the highly charged ion in a process called Charge Exchange (CX). The CX rate is proportional to the neutral background density n_0 and interaction cross-section. The latter is modelled by the Mueller & Salzborn formula [22] which predicts a higher cross-section for higher charged projectiles and a decrease for neutral targets with higher ionisation potentials.

Elastic collisions of beam electrons and trapped ions, are the main and continuous source of thermal energy. Resulting in a rising ion temperature, this process is commonly dubbed Spitzer- or Electron Heating (EH). The heating rate expression is similar to that of the inelastic charge breeding processes, but relies on the Coulomb cross-section [23] for elastic charged particle collisions. A further heating term is associated with the sudden change in potential energy as a trapped ion changes its charge state. The potential energy difference depends on the ion's radial position during the interaction and is thermalised in subsequent ion-ion collisions, hence driving temperature changes [24]. This is usually referred to as Ionisation Heating (IH).

As stated above, identical ions are assumed to be in thermal equilibrium at all times. Temperature differences between unlike ions are however permissible in this model and expected due to their differing response to the aforementioned heating mechanisms. Because these ions occupy a shared volume, they are however expected to strive towards a common temperature that is mediated by ion-ion collisions. The speed at which Thermal Relaxation (TR) occurs, and hence how strongly temperatures of differing ions are coupled, depends mostly on the ion mass and collision frequency [24].

Ion escape occurs when ions in the high energy tail of the thermal distribution obtain sufficient energy to overcome the radial space charge potential or the externally applied axial trapping potential. As these ions are lost instantaneously, there is actually an upper limit for the containable energy effectively clipping the tail, and the escape rate can be determined by evaluating the ion velocity diffusion rate at the critical value. This is an approximation method, and throughout the years various rates have been suggested. In all expressions the dominating factor is the ratio of the ion temperature

2025 JINST 20 C03053

and the trapping potential the ion is experiencing scaled by its charge. In *ebisim* the rate for escape is implemented following the model of Fussman et al. [25], which predicts somewhat larger escape rates than the expression originally put forward by Penetrante [13], cf. [12].

This description has so far largely glossed over the radial dimension, which cannot be ignored when developing a full simulation model. Due to the strong pinning of beam electrons to magnetic flux lines, it is generally assumed that the electron beam profile does not vary much during the charge breeding process. For the *ebisim* code, we therefore assume that the electron beam has a fixed current and radial size. Furthermore, this model is currently limited to uniform electron beams with homogeneous j, but may generally be expandable in the future.

The charge density of the beam provides the radial trapping field in which ions are expected to distribute themselves according to their temperature and follow a Boltzmann distribution. In this manner, the linear ion density N can be associated with a radial extent and consequently volumetric density n. Generally, some ions will be outside the edges of the electron beam, motivating the introduction of the electron ion overlap factor f_{ei} as these ions are not expected to partake in inelastic collisions with beam electrons.

As the total ionic charge in the trap is increased, the positive charge density will eventually become comparable to the electron beam's charge density. At this point, the radial potential is formed by both the fixed beam, and the dynamic ions. This is a highly non-linear problem, as the ions now diminish the very potential that keeps them trapped. In *ebisim* a fast custom finite difference solver is implemented to iteratively determine a solution to the nonlinear Poisson equation on every single evaluated time step. In addition to yielding information about the spatial ion distribution, the solution also allows one to make corrections to the space charge trap depth and the electron beam energy as the electron beam is compensated by ions.

The *ebisim* tool provides the user with the option to configure the simulation to disable one or more of mechanisms introduced above. This is helpful in assessing their relevance and emerging consequences for the charge breeding process, as equivalent experiments can usually not be carried out in practice. Additionally, disabling the custom radial solver (which is justified for low neutralisation degrees), can notably speed up the simulation as a large fraction of computation is skipped.

A secondary minimal simulation model, referred to as basic *ebisim* throughout this article, fully excludes thermal effects and CX and can produce lightweight results in a few milliseconds; this capability is exposed in a small web-app that allows running and inspecting simple charge breeding simulations within any modern web browser [26].

3 Latest charge breeding results at REXEBIS

This section presents a follow-up series of measurements conducted at REXEBIS, aimed at refining our understanding of charge breeding for heavy elements and investigating the effective electron current density $j_{\mathrm{eff}} = j \cdot f_{ei}$ for both light and heavy ions. Previous measurements have revealed that j_{eff} varies with ion species, particularly with ion mass. To further explore this behaviour, we focus on comparing the charge breeding of lighter potassium ions with that of heavier uranium ions, using the *ebisim* simulation package to analyse the breeding processes.

2025 JINST 20 C03053

3.1 Setup

The complete REX-ISOLDE charge breeder system, consisting of an accumulating, cooling, and bunching Penning trap [27] followed by the charge breeding EBIS, is described elsewhere [28]. Since 2020, REXEBIS features a non-adiabatic gun for which an extensive report on the design and commissioning is found in ref. [5]. Table 1 summarizes the main parameters of REXEBIS in its present configuration. The exact measurement process for breeding efficiencies and the instrumentation involved are detailed in section IV in the same reference.[1] It should be noted that throughout the article, the discussed charge breeding efficiencies do not include the additional losses induced by the Penning trap, which has a typical transmission of 30 to 55 %.

Table 1. REXEBIS design parameters as of 2020. Voltages are given with respect to EBIS ground potential; the r_{ebeam} value is derived from electron beam simulations; $U_{\text{outer barrier}}$ voltages are given during the trapping and injection-extraction phases.

Parameters	
B_{cathode}	0.07 T
B_{trap}	2 T
I_e	200 to 300 mA
U_{cathode}	−5500 to −7000 V
r	0.187 mm
L_{trap}	800 mm
$r_{\text{drift tube}}$	5 mm
U_{trap}	700 V
$U_{\text{inner barrier}}$	2000 V
$U_{\text{outer barrier}}$	1200 V / 0 V

For the potassium ($^{39}_{19}$K) tests, the stable 1+ beam was produced in a local surface ion source in front of REXTRAP. A DC ion beam was injected into the Penning trap, responsible for bunching and cooling. The pulsed beam ejected from REXTRAP, with a typical length of 10 µs, was transported at 30 keV via an electrostatic beam transfer section to REXEBIS. The outer barrier was temporarily lowered during the moment of injection, and rapidly closed thereafter to trap the injected bunch containing 2.8×10^6 to 7.0×10^6 ions.

For the uranium ($^{238}_{92}$U) tests on the other hand, the DC beam originated from a standard target-unit, featuring a surface ion source, installed at the front-end of the General Purpose Separator (GPS) at ISOLDE [29]. For this heavier beam, the pulse length out of REXTRAP was approximately 20 µs. Depending on the repetition rate of the charge breeder system, the beam intensity injected into REXEBIS varied between 2.6×10^6 and 4.8×10^6 ions/pulse.

The breeding time inside the EBIS dictates the shortest possible accumulation period in REXTRAP and thereby limits the repetition rate of the system. The former was varied, and the values are given below. The ions were expulsed from the EBIS by lowering the outer potential barrier fully at the end of the breeding cycle. The charge state distribution (CSD) analysis of the ion ensemble was thereafter performed in the Nier-type spectrometer in front of the linear accelerator [5]. Injected and extracted charges were measured as time-averaged currents, which are presented in the result section below.

[1] NB. In the article, the definition for the single charge state efficiency (eq. 1) is incorrect and should be read as $\eta(Q) = FC4(Q)/(FC2 \cdot Q)$.

2025 JINST 20 C03053

In the case of the potassium tests, an electron beam current of 223 mA was employed, with a beam energy of (5950 ± 50) eV (accounting for the negative space-charge depression of around 340 V inside the drift tubes). For uranium, five cases of electron beam current and energy were measured, see table 2 below. REXEBIS was operated with nominal residual gas pressure, i.e. $P_{\text{gun}} \sim 1 \times 10^{-11}$ mbar and $P_{\text{collector}} \sim 5 \times 10^{-10}$ mbar, while the electron beam was running. Despite this good base pressure, the residual gas content inside the breeding region completely dominated over the injected ions to be charge bred, in particular H and Ne, with estimated partial pressures of 3.9×10^{-11} and 1×10^{-11} mbar, respectively, during the two measurement series. Table 3 tabulates the number of injected and residual gas ions for the longest breeding times encountered during the tests. Neon is injected as a cooling gas inside REXTRAP and effuses via the transport line into the EBIS. The less abundant C, N, O and Ar make up approximately 15 % of the residual gases and were ignored in the *ebisim* simulations.

Table 2. Data from the uranium charge breeding measurement series. In columns 't_{breed} current scaled' and 'j_{est} current scaled', the respective values have been adjusted for the varying electron current, to correspond to a situation of an electron current of 245 mA, as t_{breed} (current scaled) = $t_{\text{breed}} \cdot I_e/245$ and j_{est} (current scaled) = $j_{\text{est}} \cdot 245/I_e$.

Case	I_e (mA)	U_e (eV)	t_{breed} (ms)	t_{breed} current scaled (ms)	Q_{ave}	j_{est} (Acm^{-2})	j_{est} current scaled (Acm^{-2})	Maximum single charge-state efficiency (%)	Total EBIS efficiency (%)	Neutralisation degree (%)
1	245	6130	195	195	55.1	580	580	14.0	73.3	3.5
2	245	6130	295	295	57.7	600	600	16.8	73.3	4.6
3	245	6130	395	395	59.0	580	580	17.6	71.4	5.5
4	309	6035	395	498	59.9	730	579	15.8	68.2	5.4
5	320	6540	395	516	60.6	820	628	18.2	67.4	4.7

Table 3. Number of injected metallic ions and the corresponding estimated number of hydrogen and total number of neon ions inside the trapping region at the end of the breeding cycle.

195 ms		
K	H^+	Ne^+-Ne^{10+}
5.6×10^6	8×10^7	8×10^7

395 ms		
U	H^+	Ne^+-Ne^{10+}
4.8×10^6	2×10^8	1.5×10^8

3.2 Potassium results

The measured potassium CSD for a breeding time of 195 ms (period time = 200 ms) is shown in figure 1. Even though the electron beam energy exceeded the binding energy for K^{17+}, i.e., 4610.8 eV [30], the closed-shell configuration boosts the occupancy of the 17+ charge state (the binding energy for K^{16+} is 1034.5 eV). The sum of all extracted potassium charges was 3.4 ppA (time-averaged particle-pA current). With 4.5 pA extracted from REXTRAP, that corresponds to an EBIS total efficiency of ~75 %.[2] The corresponding single charge-state efficiency predictions from *ebisim*, employing an electron current density of 191 A cm^{-2} and an ion injection temperature of 10 eV, is also indicated (parameters motivated below). The efficiency values were scaled for the measured total efficiency of 75 %. The prediction of the fully featured simulation agrees well with the measured distribution.

[2]The EBIS total efficiency is defined as the fraction of extracted to injected number of potassium ions.

2025 JINST 20 C03053

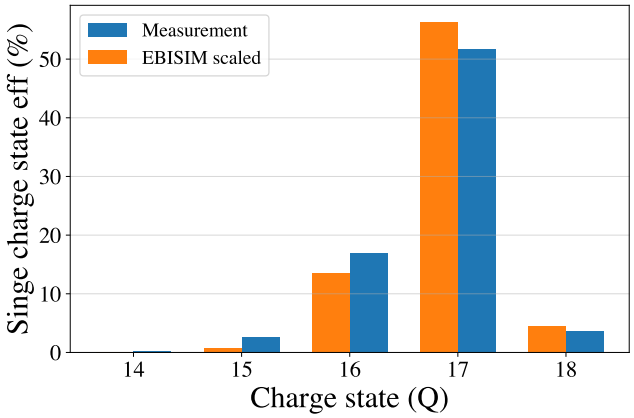

Figure 1. EBIS single charge-state efficiency for potassium charge bred for 195 ms (blue) and corresponding *ebisim*-simulated charge state abundance (orange) scaled for the total EBIS efficiency, assuming a current density of 191 A cm^{-2} and an ion injection temperature of 10 eV.

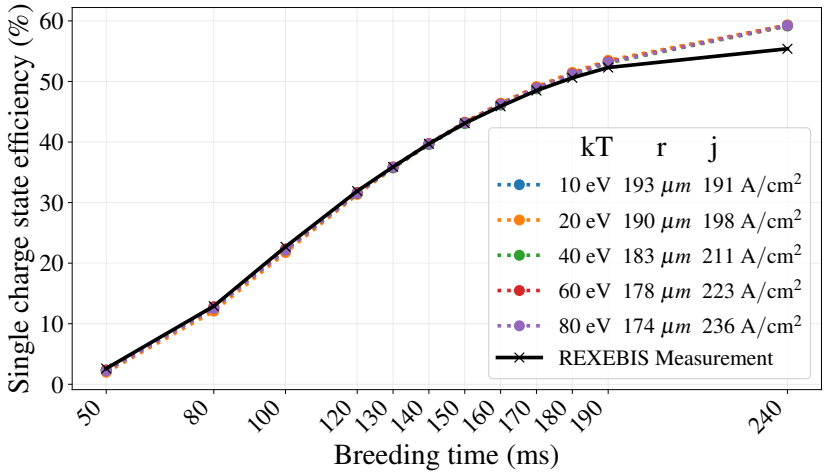

Figure 2. Single charge-state efficiency for K^{17+} as a function of breeding time. The black curve represents the measured EBIS data, and the coloured curves correspond to fitted *ebisim* simulations. Each coloured line reflects a combination of current density and injection energy that yields the best overall fit to the data.

The EBIS single charge state efficiency for K^{17+} was measured as a function of breeding time, with the results presented alongside fits from *ebisim* simulations in figure 2. Fits to the measured data were performed for simulations with increasing injection energies, where the current density for each case was varied until the abundance evolution was reproduced. As seen from these simulations, a tighter electron beam, or higher current density, is required to compensate for an increase in ion injection temperature. A slightly larger discrepancy is observed for the 240 ms breeding time data point, for which the period time had to be increased from 200 to 500 ms. It is speculated that the Penning trap efficiency dropped due to the increased number of accumulated ions, and therefore the injected current into the EBIS was overestimated for this data point.

Figure 3 presents the optimal breeding time per charge state for both the experimentally obtained data and a series of *ebisim* simulations performed with different combinations of injection energy and current density, as determined by the fittings in figure 2. The results in figure 3 demonstrate a

2025 JINST 20 C03053

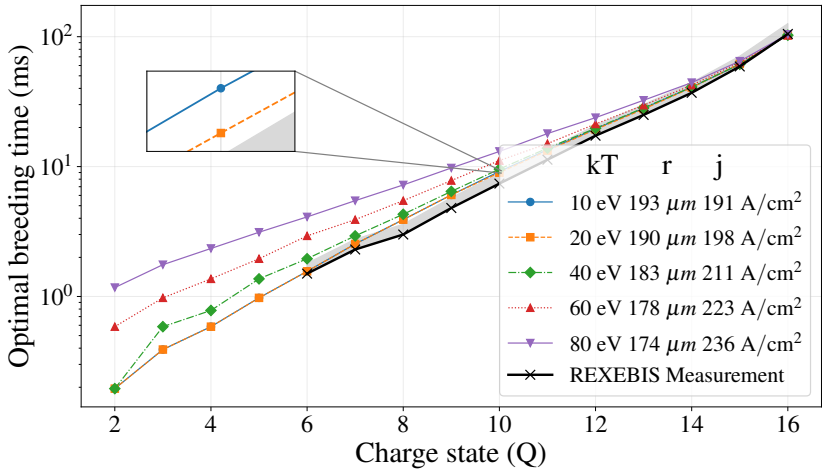

Figure 3. Semi-log plot showing optimal breeding time as a function of charge state for measured REXEBIS data (black) compared against *ebisim* simulations with varying combinations of injection energy and current density (coloured). A non-symmetrical systematic measurement error of 20 % is indicated by gray shading. The zoomed inset aids in distinguishing the close-laying curves obtained for simulations performed with the lowest injection energies.

progressively poorer fit as the injection energy and current density increase. Low injection energy simulations with kT = 10 and 20 eV, and j = 191 and 198 A cm^{-2}, show some deviations from the measured data for K^{7+} to K^{12+} but offer the overall best fit. Accounting for a one-sided systematic error (20 %) also yields kT = 40 eV with j = 211.0 A cm^{-2} as a good fit. The almost perfect exponential increase in breeding time with charge state is striking, suggesting an effective electron current density not varying with the charge state.

Finally, the REXEBIS single charge-state efficiencies for K^{6+} to K^{17+} were recorded and are displayed in figure 4. The very low efficiency for charge states 6+, 7+, and 8+, followed by a sharp increase at 9+, has been observed previously [5].

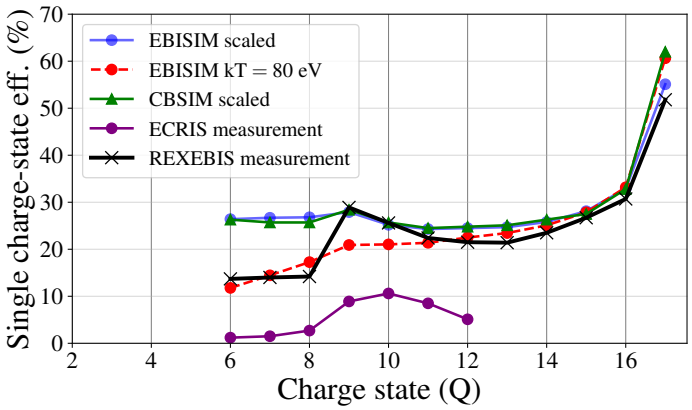

Figure 4. Single charge-state efficiencies for potassium: REXEBIS measurement (black curve); *ebisim* prediction for REXEBIS parameters scaled with the total efficiency (blue curve); CBSIM prediction for REXEBIS parameters scaled with the total efficiency (green curve); *ebisim* prediction for REXEBIS parameters including an ion injection temperature of 80 eV (red curve); and ECRIS measurement data [31] (purple curve).

2025 JINST 20 C03053

3.3 Results from uranium

The measurement series for uranium charge breeding was carried out in a different manner. For three different breeding times, the full uranium charge state distributions were recorded, which improves the reliability of the analysis. Moreover, the total extracted current was recorded for each breeding time, such that the beam neutralisation could be determined. On the other hand, the electron beam parameters were changed in some cases, which complicates the interpretation. The complete set of data points, with detailed electron beam parameters, is given in table 2. A typical uranium charge state distribution, corresponding to case 4 in table 2, is presented in figure 5.

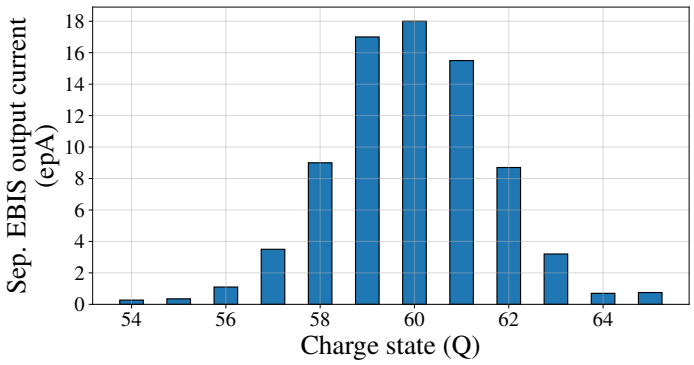

Figure 5. Extracted time-averaged uranium current in different charge states after 395 ms breeding time inside a 309 mA electron beam with an energy of 6035 eV.

The average charge states for 195, 295 and 395 ms breeding time in a 245 mA electron beam are plotted in figure 6, together with data points recorded in 2006 using the original electron gun. The earlier data was recorded with a lower electron current of only 174 mA. Hence, to perform a comparison, those breeding times were linearly scaled to an electron current of 245 mA. The derived electron current density for the original gun, after scaling, is $(144 \pm 12)\,\mathrm{A\,cm^{-2}}$ ($1\,\sigma$). The dashed horizontal line indicates the minimal charge state accepted by the room-temperature section of the LINAC for acceleration of ^{238}U, demonstrating that this heavy beam can now be post-accelerated to the experimental setups.

From each of the five uranium data points the most abundant charge state can be selected. The EBIS single charge state efficiencies, as well as total efficiencies for these charge states, are plotted in figure 7, with average values amounting to (16.5 ± 1.5) % ($1\,\sigma$) and (70.7 ± 2.5) % ($1\,\sigma$). These single charge state efficiencies are not maximal, as the breeding times were not selected to optimise specific charge states. Nevertheless, note that the efficiencies are almost independent of the charge state.

For the 320 mA electron current, an apparent effective electron current density as high as $628\,\mathrm{A\,cm^{-2}}$ was achieved. To allow for comparison between breeding times and electron current densities despite varying electron currents, both entities were scaled to an electron current of 245 mA (columns 5 and 8 in table 2). Thereafter, the respective electron current densities could be derived making use of *ebisim*. The scaled current density as a function of the average charge state is plotted in figure 8, with an average value of $(593 \pm 19)\,\mathrm{A\,cm^{-2}}$ ($1\,\sigma$). No reduction in current density is observed with increasing charge state or breeding time.

The uranium ions only make up a small fraction of the total ion space charge, which is dominated by lighter ions, such as hydrogen, carbon, nitrogen, oxygen and argon. In fact, approximately 12 % of the extracted beam current stems from uranium ions, and in terms of number of ions only approximately 1 %.

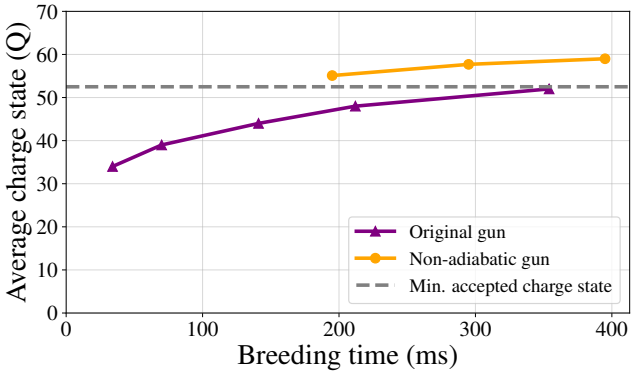

Figure 6. Attainable abundance-weighted average charge state for uranium as a function of breeding time for the non-adiabatic electron gun (orange trace), and the original electron gun (purple trace; data recorded 2006). The breeding times for the original electron gun were scaled to an electron current of 245 mA.

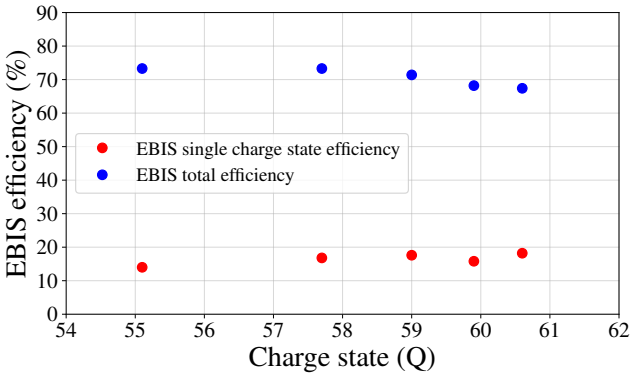

Figure 7. EBIS single charge-state efficiency (non-optimised) (blue) and EBIS total efficiency (red) as function of charge state for the five uranium data points in table 2. The dots, from left to right, correspond to cases 1 to 5.

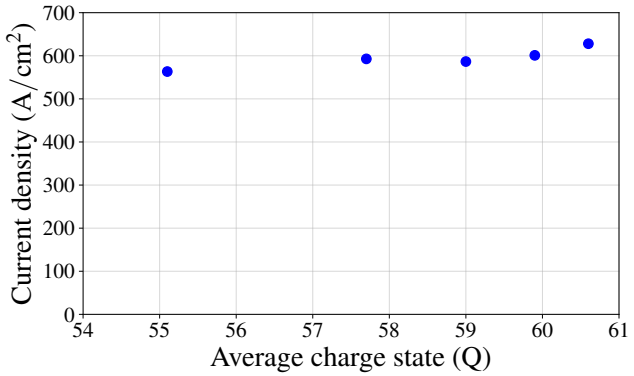

Figure 8. Effective electron current density derived from the five charge-state distributions, after the varying electron current was scaled to a current of 245 mA. The dots, from left to right, correspond to cases 1 to 5 in table 2.

2025 JINST 20 C03053

3.4 Charge breeding discussions

3.4.1 Potassium

Using the measured data for K^{9+} to K^{17+} in combination with the abundance predictions from *ebisim*, we have again demonstrated that the REXEBIS total efficiency is around 75 %. Due to limitations in the beam instrumentation, we cannot determine the exact location of the 25 % loss: it may take place either in the beam transfer section between the Penning trap and the EBIS, upon injection into the actual EBIS, or during the extraction process through the A/Q-separator. We assume the loss is not occurring during the actual breeding process, as we do not record any variation in total efficiency with the breeding time.

It is encouraging to note that such high charge state as K^{17+} can be achieved, in combination with a single charge state efficiency of 55 %. From a beam-delivery point of view, however, the long breeding time of ~200 ms should be compared to around only 8 ms, which is required to reach 10+ (i.e. A/Q < 4) with a single charge-state efficiency of around 25 %. Due to an electron beam energy exceeding the ionisation threshold for K^{17+}, also some K^{18+} is produced.

The basic version of *ebisim* assumes a full overlap between the ion population and the electron beam and considers only electron-ion impact ionisation, radiative recombination and dielectric recombination in the charge breeding process. The advanced *ebisim*, however, can include additional effects such as charge exchange, heating effects, collisional thermalisation and escape mechanisms. To examine the impact of these effects, a series of simulations on potassium were performed, sequentially incorporating more processes in the advanced *ebisim* code. The simulated distribution in figure 1 served as a reference. The breeding time required to reproduce this reference charge-state distribution was recorded for each progressively more comprehensive simulation model, beginning with only electron-ion impact ionization. These measurement series were repeated for ion injection energies of 10 and 80 eV to asses the impact of varying starting conditions. The results are presented in table 4, where it can be seen that the breeding time for potassium is slightly longer when a non-zero ion injection temperature is assumed, indicating a reduced overlap factor. When heating mechanisms are included, the required breeding time increases significantly for the $T_{\mathrm{inj}} = 80$ eV case due to a further reduction in the overlap factor. However, once thermal relaxation is activated, the breeding time decreases again. We conclude that the residual gas pressure is sufficiently high to absorb excess energy of the potassium ions once the heating and TR mechanisms are incorporated, without necessarily allowing for boil-off of the residual gas ions. At the same time, the pressure is low enough not to hamper the breeding process via charge exchange or neutralisation effects.

As demonstrated in figure 4, neither *CBSIM* [32], which applies a simpler model for the calculation of the binding energies used in Lotz's formula nor *ebisim*, reproduces the efficiency step for potassium when going from K^{8+} to K^{9+}, but both models produce similar results. It is interesting to note that a similar efficiency step, going from 2.7 to 8.9 %, has been observed in an ECRIS charge breeding device operating with an injected potassium beam [31], where the containment conditions, electron temperature and distribution, and residual gas pressures are quite different, see figure 4. The abundance prediction from *ebisim*, based on the derived current density, is plotted after scaling for the total EBIS efficiency. As noted, the steep efficiency increase at charge state 9+ is not captured by the model. Introducing an initial temperature of injected potassium ions, such as 80 eV, suppresses the abundance of lower charge states in the *ebisim* simulations. This is due to the reduction of the electron-ion overlap factor, resulting in a slower feeding of 1+ ions into the stepwise ionisation process.

2025 JINST 20 C03053

Table 4. Breeding times required to reproduce the measured charge-state distribution for potassium after including various phenomena in the simulations. The column heading specifies what effect was added to the already listed columns to the left. The breeding times are given for two assumed 1+ ion injection energies, 10 eV (i.e. in principle fully immersed within the electron beam) and 80 eV.

T_{inj}	EI	RR+DR	CX	EH + IH	TR	Escape	Radial dynamics
10 eV	0.1938 s	0.1940 s	0.1944 s	0.2039 s	0.1950 s	0.1950 s	0.1950 s
80 eV	0.1972 s	0.1975 s	0.1984 s	0.2612 s	0.2019 s	0.2019 s	0.2020 s

EI: Electron-ion impact ionisation, RR: Radiative recombination, DR: Dielectronic recombination, CX: Charge exchange, EH: Electron heating, IH: Ionisation heating, TR: Thermal relaxation.

While a higher initial temperature better replicates the efficiency for charge states 6+ to 8+, it fails to capture the sharp transition from K^{8+} to K^{9+} and conflicts with the results in figure 3, which show progressively poorer fits with increased temperature.

Determining the initial ion temperature is challenging due to multiple plausible injection temperatures explaining the data in figure 3 and inherent uncertainties in *ebisim*, particularly early on in the breeding cycle due to its inability to capture the K^{8+} to K^{9+} efficiency step. Given the measured injection >200 eV above the bottom of the electron beam potential, one would expect higher temperatures than kT = 10 and 20 eV. However, for longer breeding times, the simulations become less sensitive to these initial conditions and *ebisim* proves effective in predicting the electron current density. From comparing the final charge state distributions in figure 1, an electron current density of 191 A cm^{-2} was derived, translating into a radius of a uniform electron beam of 193 µm, which is in good agreement with 187 µm given by electron beam simulations [5]. Nonetheless, this is in strong contrast to the current density prediction from the uranium data, as presented in the next section.

3.4.2 Uranium

Before continuing the comparison of the predicted electron current densities, let us first investigate how additional processes affects the charge breeding time for uranium in case 4 of table 2 by applying the same method as for potassium in table 4. The results are shown in table 5. The simulations were performed with a current density of 731 A cm^{-2} (corresponding to an electron beam radius of 116 µm), which best reproduced the charge state distribution while using the basic *ebisim* model. Due to the proximity of the electron beam energy to the ionisation potential (3827 eV for U^{59+}), the effect of the RR is noticeable. As for the potassium case, the breeding time is extended with the heating processes enabled, but once TR is included — allowing the hot uranium ions to share their energy with the colder residual gas ions — the ion cloud is again confined within the electron beam and the breeding time is lowered. Furthermore, one concludes that the injection energy does not affect the required breeding time. The reason is that an increased ion injection energy only affects the electron-ion overlap for the first few charge states before the ions are well trapped within the electron beam, and as the stepwise ionisation time is then $\ll$1 ms, the overall effect on the charge-state distribution is insignificant. Even with all effects accounted for, the current density for uranium is very high, and linearly scaled with the electron current from 309 mA to 223 mA (the reference current for the potassium tests), one arrives at 528 A cm^{-2}, i.e. approximately a factor 2.8 higher than for potassium.

2025 JINST 20 C03053

Table 5. Breeding times required to reproduce the measured charge state distribution for uranium after including various phenomena in the simulations. The column heading specifies what effect was added to the already listed columns to the left. The breeding times are given for two assumed 1+ ion starting energies, 10 eV (i.e. in principle fully immersed) and 80 eV.

T_{inj}	EI	RR+DR	CX	EH + IH	TR	Escape	Radial dynamics
10 eV	0.3542 s	0.4067 s	0.4067 s	not reached	0.4103 s	0.4100 s	0.4100 s
80 eV	0.3542 s	0.4070 s	0.4075 s	not reached	0.4104 s	0.4101 s	0.4101 s

EI: Electron-ion impact ionisation, RR: Radiative recombination, DR: Dielectronic recombination, CX: Charge exchange, EH: Electron heating, IH: Ionisation heating, TR: Thermal relaxation.

The evolution of the uranium, neon and hydrogen ion temperatures is given in figures 9(a), 9(c) and 9(e), showing a rapid increase in temperature for the lower uranium charge states, caused by IH. At around 2 ms, the highly charged neon ions start exchanging energy with the hot uranium ions, such that their temperature is reduced to ~180 eV at the end of the breeding cycle. One also notices that around 7 ms, all charge states of the uranium ions are thermalised. For $Ne^{8+,9+,10+}$, this occurs 40 ms into the breeding cycle, and their temperature is similar to that of the uranium ions. The hydrogen ions, on the other hand, never attain the same energy due to the lower interaction cross-section and unfavourable mass ratio to the heavier neon and uranium.

The charge-state abundances as a functions of time are presented in figures 9(b), 9(d) and 9(f). A higher single charge state efficiency is predicted when approaching U^{60+}, caused by the proximity to the Ar-like closed-shell at U^{64+}. A careful inspection of the line representing the H^+ linear density will show a slight deviation from a straight line, indicating an escape of ions from the system. Such a deviation cannot be noticed for the neon ions, nor for the total amount of uranium ions. The radial distribution functions, shown in figure 10, provide further evidence for a certain radial loss of hydrogen ions as the abundance tail, even though small, is non-negligible at the drift tube radius (5 mm). Actually, in this particular case, the outer barrier of 500 V coincides with the radial voltage depression, so the losses most probably occurred in the axial direction, where no magnetic field enhances the effective radial holding force on the ions.

The effect of the trapped ion charge states on their radial distribution is well demonstrated with the uranium and hydrogen ions. In spite of the latter 1+ ensemble having a lower temperature, the radial reach is longer than that for the highly charged uranium ions that are tightly bound to the electron beam axis. The required holding voltage for U^{60+} is on the order of $200/60 = 3.3$ V, while for H+ as high as 58 V. These voltages should be compared to the potential depth of the electron beam, which amounts to 60 V. In fact, as seen in figure 11, 75 % of U^{60+} resides within 30 µm of the beam axis, i.e. reaching only a fraction of 0.26 of the simulated electron beam radius. In comparison, the potassium ions are less tightly bound to the beam axis. Figure 12 shows the cumulative distribution of potassium ions simulated for 195 ms breeding time. Here, 75 % of K^{17+} resides within 80 µm of the beam axis, which translates to a fraction of 0.40 of the simulated electron beam radius. Thus, a strongly non-uniform electron beam, with a very high density near the centre, could possibly explain the observed difference in electron current density between potassium and uranium. The present version of *ebisim* does not feature the possibility to model non-uniform electron beams, so the assumption has not been verified.

2025 JINST 20 C03053

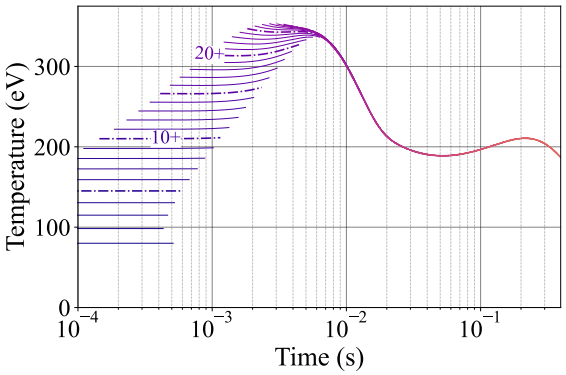

(a) $^{238}_{92}U$ temperature

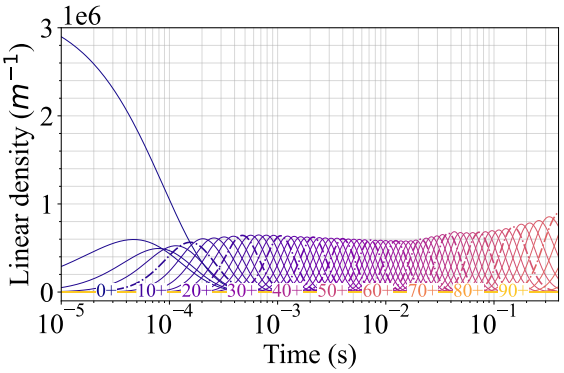

(b) $^{238}_{92}U$ charge states

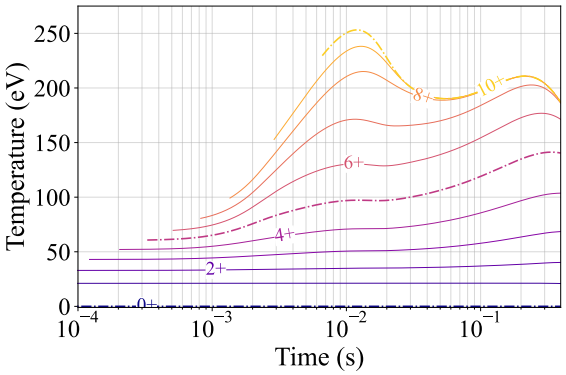

(c) $^{20}_{10}Ne$ temperature

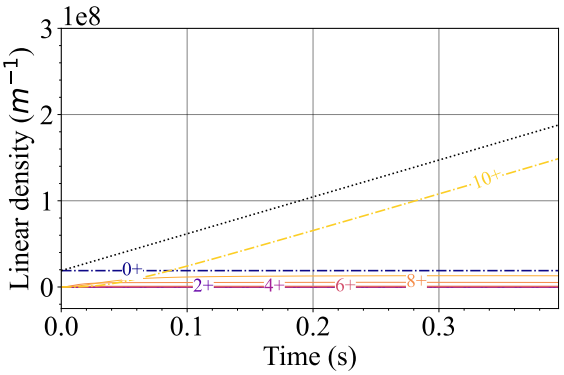

(d) $^{20}_{10}Ne$ charge states

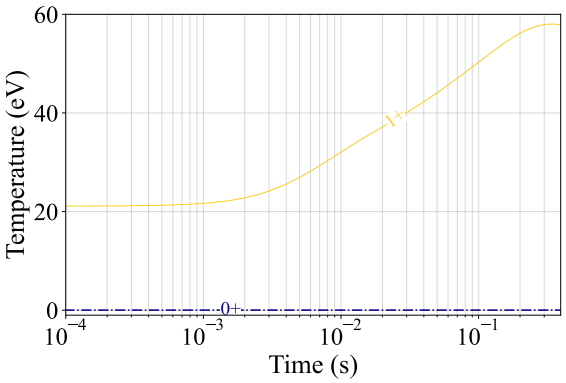

(e) $^{1}_{1}H$ temperature

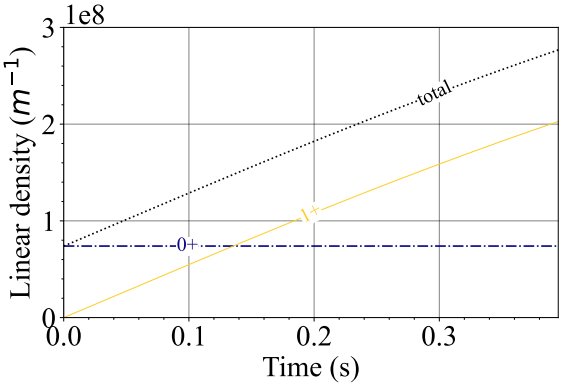

(f) $^{1}_{1}H$ charge states

Figure 9. (Left column) Simulated ion temperature evolution during the uranium breeding test (case 4). The temperatures of the individual charge states are only indicated during the time-period where their linear density is higher than 1×10^4 ions m^{-1}. (Right column) Simulated linear densities for uranium, neon and hydrogen as function of breeding time. The dashed lines indicated the total number of the element, including neutrals.

2025 JINST 20 C03053

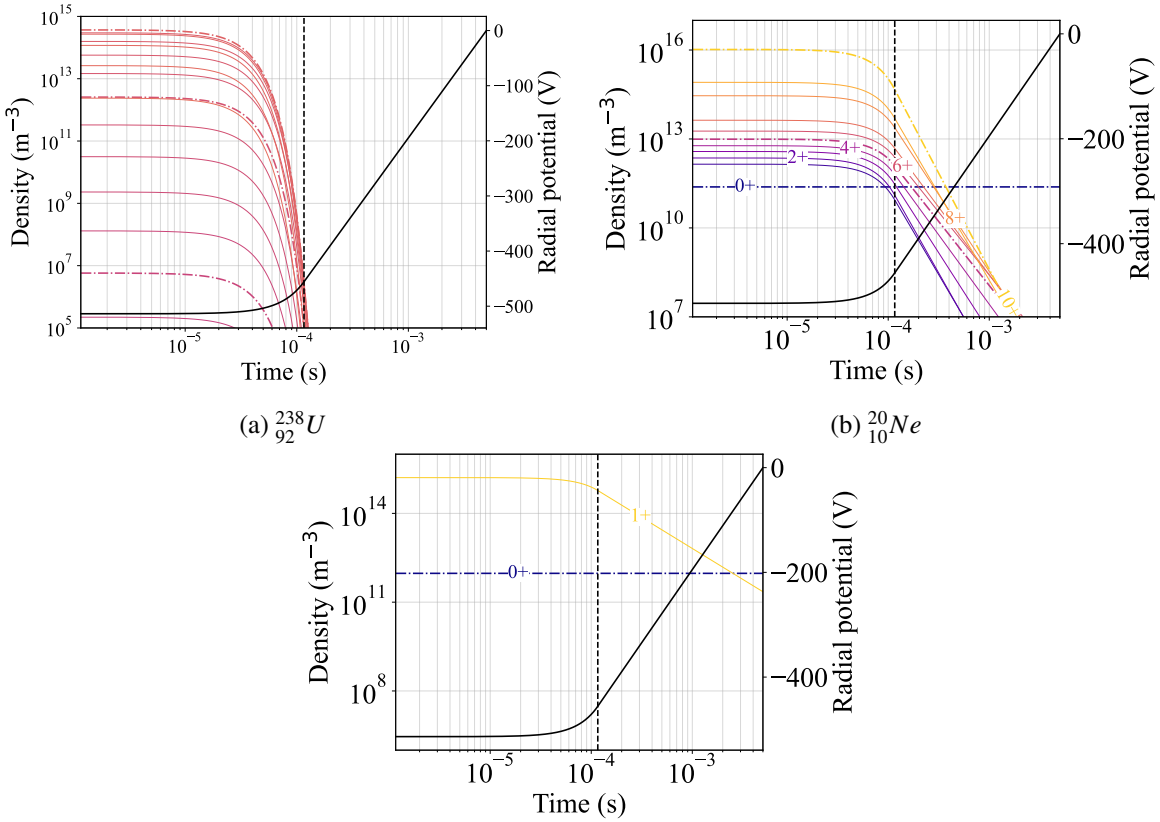

(a) $^{238}_{92}U$ (b) $^{20}_{10}Ne$

(c) $^{1}_{1}H$

Figure 10. Simulated radial distributions of the uranium and residual gas ions, out to the drift tube radius of 5 mm. The full black line indicates the space charge potential with respect to the drift tube. The vertical dashed line indicates the electron beam radius, in this case assumed to be 116 µm such that an electron current density of 731 A cm^{-2} is attained.

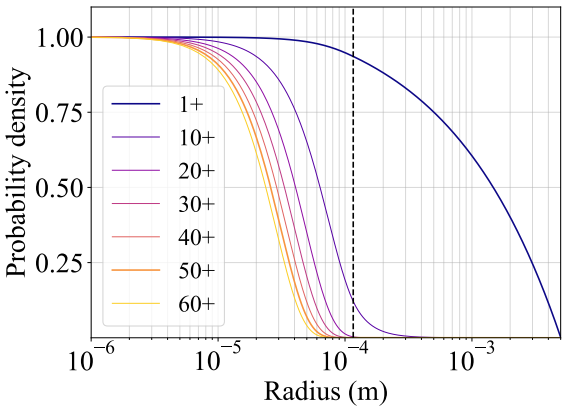

Figure 11. Cumulative radial distribution $^{238}_{92}U$.

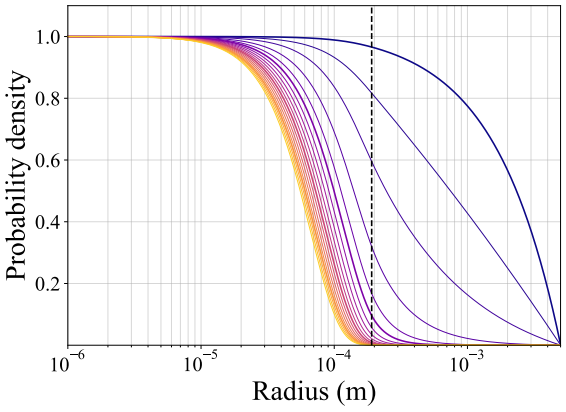

Figure 12. Cumulative radial distribution $^{39}_{19}K$.

During the initial commissioning of the non-adiabatic electron gun, the electron current density was measured for a set of different elements, stretching from ^{7}Li to ^{152}Sm. A clear trend towards higher current densities for the more highly charged elements was found. In addition, a decrease in the current density with breeding time was observed, which is not the case for the uranium series in this paper. However, it should be pointed out that the evaluation process for the current density was different in ref. [5] (see section D.1), compared to the simpler model applied in this paper. The effective electron current density deduced from a potassium measurement during commissioning was around 200 A cm^{-2} for a 200 mA electron beam, which supports the recent results.

While some semi-empirical formulas for multiple-ionisation cross-sections are proposed in the literature [33], they are not yet part of the *ebisim* package. In any case, an electron beam energy limited to 6035 eV prevents double-ionisation beyond charge states above U^{51+}. Since approximately 80 % of the breeding time is spent in charge states above this threshold, the remaining contributions from double- and multiple-ionisations on the charge state evolution would not be enough to account for the large discrepancy between required breeding times observed.

3.4.3 Ionisation cross-section models

In our current model (see section 2), successive ionisation is driven only via direct EI with cross-sections determined using the Lotz formula coupled with binding energies obtained from the Flexible Atomic Code (FAC) [14, 34]. Here, we compare the EI cross-sections obtained using the Lotz formula against those obtained from the Binary Encounter Bethe (BEB) model, Binary Encounter Dipole (BED) model, Coloumb-Born (CB) model and the Distorted Wave (DW) model, all included as options in FAC. Ionisation from all energetically available subshells were considered and the presented cross-sections reflects the sum of all subshell contributions. Moreover, the cross-sections were evaluated on a 100 point grid of incident electron energies in the range 5000 to 7000 eV, from which cross-sections at specific energies could be interpolated.

To assess the impact of applying different EI cross-section models, the single charge-state efficiency simulation shown in figure 4 were repeated with Lotz's formula exchanged for each of the above-mentioned models. Thus, the results are presented in figure 13 and cross-section ratios are shown in figure 14. For potassium at an incident electron energy of 5965 eV, the Lotz formula consistently produces the highest cross-sections among the tested models. The largest cross-section ratios are observed at the lowest charge states but have minimal impact on the single charge state efficiency simulations due to rapid ionisation early in the breeding cycle. Note that the single charge-state efficiency for K^{17+} is not maximised due to the limited breeding time and, the presented values therefore depend on the chosen cross section model and can be ignored for this discussion. The poor replication of measured single charge-state efficiency for the lower charge states is not improved by any of the other models.

3.4.4 Collisional excitation — autoionisation

A similar investigation into different EI models for uranium did not show any significant impact on the charge breeding simulations. To explain the apparent high electron current density for uranium, we therefore explored an additional ionisation channel via Collisional Excitation (CE) followed by AutoIonisation (AI). The cascade process of CE followed by AI will be referred to as AE. The preliminary estimates below aim to provide a general understanding of the potential contributions from AE to the total ionisation cross-section.

2025 JINST 20 C03053

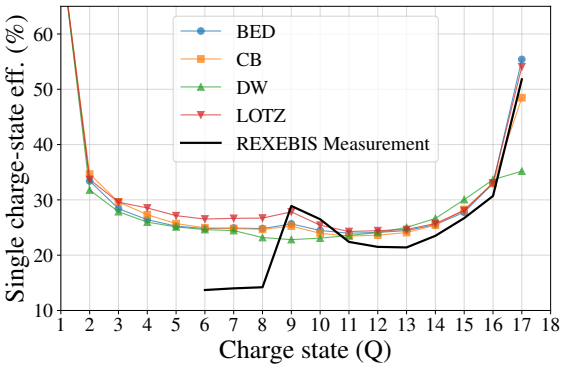

Figure 13. Single charge-state efficiency as a function of the charge state for potassium. The REXEBIS measurement (black solid line) is compared with *ebisim* simulation results (coloured lines) using different EI models.

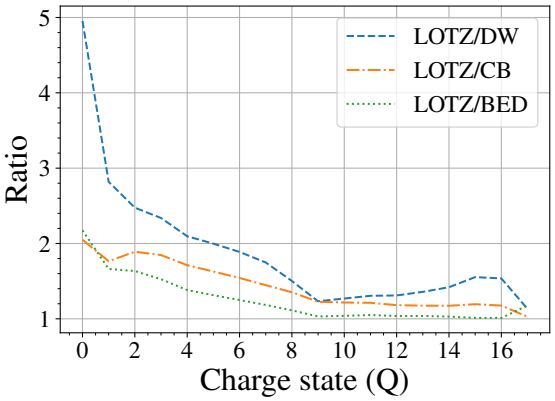

Figure 14. Potassium ionisation cross-section ratios calculated using the Lotz formula with those predicted by various models at an incident electron energy of 5965 eV.

The CE cross-sections were computed using a scattered-electron energy grid within the FAC code, with interpolation applied to determine the cross-sections at relevant incident electron energies. The calculations focused exclusively on excitations from the ground state configurations of U^{x+}, where $x = 54, 55, \ldots, 59$, since more than 80 % of the breeding time is spent at these ionisation steps. The initial configurations are presented in table 6. To reduce the complexity, excitations to states below or within the valence shell were not considered. While omitting these excitations results in an underestimation of the total CE cross-section, these states predominantly decay radiatively and can therefore be excluded from this analysis. Table 7 presents the number of calculated transitions for each ion along with CE cross-sections.

Collisionally excited states either decay radiatively through photon emission or non-radiatively via the Auger process AI, which results in electron emission. The fraction of de-excitations resulting in electron emission is referred to as Auger yield. The branching ratio between the two de-excitation processes has not been computed at this stage. Instead, we impose different assumed AI transition rates, or Auger yields, artificially. This was done by scaling the computed CE cross-section by the assumed Auger yield before incorporating them to the direct EI cross-section in *ebisim*. The total ionisation cross sections was expressed as:

$$\sigma_{\text{tot}} = \sigma_{\text{EI}} + \sigma_{\text{CE}} \cdot \frac{A}{100} \tag{3.1}$$

where σ_{EI} is the EI cross section obtained using Lotz formula, σ_{CE} is the collisional excitation cross section and A is the Auger yield.

A more rigorous treatment of the total AE cross-section for U^{57+} case, performed by another group, yielded a value of 7.9×10^{-21} cm^2 at an incident electron energy of 6000 eV [35]. This value was derived from a total CE cross-section of 4.78×10^{-19} cm^2 and an Auger yield of 1.6 %. Our CE cross-section result for U^{57+} is almost a factor 13.5 smaller than the above mentioned result. We believe that this is due to the omission of excitations below and to the valence band. It is therefore realistic to assume that the amount of AI transitions from our considered excited states are larger than the 1.6 % obtained in the earlier calculations. For example, arriving at a total AE cross-section of 7.9×10^{-21} cm^2,

2025 JINST 20 C03053

from the CE cross-section presented in table 7, would entail ~20 % of the excited states decaying via AI. It is therefore within reason to assume a high percentage of AI transitions in our calculations.

Estimates of j for case 4 of uranium in table 2 are presented in table 8. It is interesting that accounting for AE for only six charge states of uranium can have such a significant impact on the estimated current density, even for relatively small AI transition rates. This result is intriguing and suggests that more rigorous calculations should be made, considering more excitation channels and fully determined branching ratios between transitions. Moreover, these cascade processes might give valuable insight into why heavy ions exhibit such apparent high electron current densities.

Table 6. Initial electronic configurations for each considered uranium ion.

U ion	Initial Configuration
U^{54+}	[Kr] $4d^2$
U^{55+}	[Kr] $4d^1$
U^{56+}	[Kr]
U^{57+}	[Ar] $4s^2$ $3d^{10}$ $4p^5$
U^{58+}	[Ar] $4s^2$ $3d^{10}$ $4p^4$
U^{59+}	[Ar] $4s^2$ $3d^{10}$ $4p^3$

Table 7. Summary of uranium CE cross-section calculations at an incident electron energy of 6000 eV. The column "# of transitions" presents the number of computed transitions with non-zero cross-sections. The last two columns show the direct electron-impact ionisation cross-section calculated using the Lotz formula and the present CE cross-section calculation.

U ion	# of transitions	Lotz EI cx [cm^2]	Coll. exc. cx [cm^2]
U^{54+}	359147	1.14E-20	1.86E-19
U^{55+}	15194	9.37E-21	3.99E-20
U^{56+}	546	7.45E-21	1.78E-20
U^{57+}	6879	6.00E-21	3.54E-20
U^{58+}	38099	4.67E-21	8.39E-20
U^{59+}	41757	3.48E-21	7.98E-20
Total	460341		

Table 8. Estimated j from *ebisim* simulations for varied AE contributions. The AI transitions reflects the percentage of transitions leading to ionisation from the considered excited states.

AI transitions	j
0 %	763 A cm^{-2}
1 %	715 A cm^{-2}
5 %	626 A cm^{-2}
10 %	579 A cm^{-2}
20 %	513 A cm^{-2}
50 %	439 A cm^{-2}

2025 JINST 20 C03053

4 Conclusions

Our experiments have demonstrated that very high charge states of injected potassium can be attained, in fact a He-like configuration, with a high breeding efficiency because of the closed-shell effect. Fully stripped potassium is energetically allowed, as the electron beam energy is approximately a factor 1.3 higher than the ionisation energy of most bound electrons, although it would entail breeding times >1 s. In general, the longer breeding times required to reach closed-shell configurations with high efficiencies may limit its practical use. The A/Q-limit of 4.5 (lately A/Q<4), set by the REX-ISOLDE LINAC, excludes the n=3 closed-shell in the Z-range around xenon, that would otherwise be reachable within an acceptable breeding time, though with a low electron beam energy that requires a special setting up of the EBIS [6]. With an upgraded LINAC accepting beams up to A/Q=6, full use of closed-shell breeding could be applied also to medium heavy nuclei. For uranium with A = 238, a peak charge state of 60+ corresponding to A/Q = 3.97, has been reached with an acceptable breeding time of ~400 ms. Previously reported total REXEBIS efficiencies of approximately 75 % were confirmed. For the production of high charge states ions of both potassium and uranium type, the breeding process was shown to be efficient without time-dependent ion losses. It should be stated that in both cases the number of injected ions was small, leading to minimal space-charge effects even for longer breeding time.

Throughout the charge breeding analysis, *ebisim* has provided useful guidance and demonstrated its potential. For example, it reproduces the single charge-state efficiency with excellent accuracy. Apart from presenting the time-dependent abundance plots, the radial particle distributions showing the overlap between the electron beam and the ion clouds can give insights into the space-charge dependence of the electron current density. Moreover, the temperature progression graphs in the uranium case showed the cooling effect from the lighter ions, necessary to obtain a uranium population well-centred along the beam axis, where the current density is believed to be the highest.

At the same time, the simulations do not predict the charge breeding efficiency of low-charged potassium ions satisfactorily, in particular near the Ne-like closed shell. Alternatives to the Lotz formula for the EI do not resolve the discrepancy. It is noteworthy that the jump in efficiency from K^{8+} to K^{9+} is also observed for ECRIS 1+ ion-injection, suggesting the effect is not machine-dependent.

Using *ebisim* on the potassium data, an electron current density of 191 A cm^{-2} could be established, well in line with the original electron beam simulations. On the other hand, the measured breeding times at REXEBIS for highly charged uranium ions implies an unexpectedly high electron density. Other groups have reported results with similarly high densities for medium-Z nuclei, exceeding the predictions from electron beam simulations [6, 7]. Thus, the anomaly is not solely connected to uranium ions and the REXEBIS setup, or the measurement method as such. Furthermore, the possibility of ions not being expelled at extraction but lingering inside the trapping region for more than one breeding cycle, thereby experiencing an effective longer breeding time that reflects itself as a higher electron current density, can be ruled out as in ref. [6], the electron beam is switched off after each breeding cycle, forcing any remaining ions to be expelled. Even though we suspect that the density profile of the electron beam is not homogeneous as assumed in the model, but peaking at the centre, in combination with *ebisim* indicating that the uranium ions are tied closer the electron beam axis than the potassium, the difference in radial distribution is not significant to boost the effective current density for the uranium with a factor 2.8 compared to potassium.

Moving forward, we will continue to build upon *ebisim* to support the analysis of charge breeding as it has already proven to be a powerful tool. Exchanging Lotz's formula for other EI models has

2025 JINST 20 C03053

shown no significant impact on the current density. Nevertheless, estimates suggest that AE may act as a contributing ionisation channel for highly charged uranium and thereby may provide an explanation for these observed high electron current densities. These findings are compelling and highlight the need for more rigorous calculations, including consideration of all available excitation channels and fully resolved branching ratios. Additionally, the observed efficiency step going from K^{8+} to K^{9+} remains unsolved but might indicate a much more rapid charge breeding process for charge states < 8+ than currently assumed. Future studies into contributing ionisation processes such as electron-ion impact double-ionisation might therefore be of interest.

References

[1] F. Ames and F. Wenander, *The REX-ISOLDE Facility*, CERN-2005-009 (2005).

[2] Y. Kadi et al., *Post-accelerated beams at ISOLDE*, *J. Phys. G* **44** (2017) 084003.

[3] F. Wenander, *Charge breeding of radioactive ions with EBIS and EBIT*, 2010 *JINST* **5** C10004.

[4] A. Pikin, H. Pahl and F. Wenander, *Method of controlling the cyclotron motion of electron beams with a nonadiabatic magnetic field*, *Phys. Rev. Accel. Beams* **23** (2020) 103502.

[5] H. Pahl et al., *Nonadiabatic electron gun at an electron beam ion source: Commissioning results and charge breeding investigations*, *Phys. Rev. Accel. Beams* **25** (2022) 013402.

[6] R. Vondrasek, ANL US, private communication (2024).

[7] A. Lapierre, MSU US, private communication (2024).

[8] M. Guerra, F. Parente and J.P. Santos, *Electron impact ionization cross sections of several ionization stages of Kr, Ar and Fe*, *Int. J. Mass Spectrometry* **348** (2013) 1.

[9] R.A. Falk et al., *Excitation-Autoionization Contributions to Electron Impact Ionization*, *Phys. Rev. Lett.* **47** (1981) 494.

[10] D.H. Crandall et al., *Electron-impact ionization of B^{2+} and O^{5+}: Excitation-autoionization in Li-like ions*, *Phys. Rev. A* **34** (1986) 1757.

[11] H. Pahl, *ebisim*, (2024), https://orcid.org/0000-0003-0498-1339.

[12] H. Pahl, *Advances in the design, modelling and operation of high-performance Electron Beam Ion Sources*, Ph.D. Thesis, Ruprecht-Karls-Universität Heidelberg (2024).

[13] B.M. Penetrante et al., *Evolution of ion-charge-state distributions in an electron-beam ion trap*, *Phys. Rev. A* **43** (1991) 4861.

[14] W. Lotz, *An empirical formula for the electron-impact ionization cross-section*, *Z. Phys.* **206** (1967) 205.

[15] W. Lotz, *Electron-impact ionization cross-sections and ionization rate coefficients for atoms and ions from hydrogen to calcium*, *Z. Phys.* **216** (1968) 241.

[16] W. Lotz, *Electron-impact ionization cross-sections and ionization rate coefficients for atoms and ions from scandium to zinc*, *Z. Phys. A* **220** (1969) 466.

[17] W. Lotz, *Electron-impact ionization cross-sections for atoms up to Z = 108*, *Z. Phys. A* **232** (1970) 101.

[18] R. Mertzig, *Project Ion Potentials*, (2015), http://project-ionpotentials.web.cern.ch/.

[19] M. Gryziński, *Classical Theory of Atomic Collisions. 1. Theory of Inelastic Collisions*, *Phys. Rev.* **138** (1965) A336.

2025 JINST 20 C03053

[20] M. Gryziński, *Two-Particle Collisions. 2. Coulomb Collisions in the Laboratory System of Coordinates*, *Phys. Rev.* **138** (1965) A322.

[21] Y.S. Kim and R.H. Pratt, *Direct radiative recombination of electrons with atomic ions: cross-sections and rate coefficients*, *Phys. Rev. A* **27** (1983) 2913.

[22] A. Müller and E. Salzborn, *Scaling of cross sections for multiple electron transfer to highly charged ions colliding with atoms and molecules*, *Phys. Lett. A* **62** (1977) 391.

[23] P. Helander and D.J. Sigmar, *Collisional Transport in Magnetized Plasmas*, Cambridge Monographs on Plasma Physics, Cambridge University Press (2005).

[24] F. Currell and G. Fussmann, *Physics of electron beam ion traps and sources*, *IEEE Trans. Plasma Sci.* **33** (2005) 1763.

[25] G. Fussmann, C. Biedermann and R. Radtke, *EBIT: An Electron Beam Source for the Production and Confinement of Highly Ionized Atoms*, in *Advanced Technologies Based on Wave and Beam Generated Plasmas*, H. Schlüter and A. Shivarova, eds., (Dordrecht), Springer Netherlands (1999) [DOI:10.1007/978-94-017-0633-9].

[26] H. Pahl, *ebisim*, (2021), http://ebis.web.cern.ch/.

[27] F. Ames et al., *Cooling of radioactive ions with the Penning trap REXTRAP*, *Nucl. Instrum. Meth. A* **538** (2005) 17.

[28] F. Wenander et al., *REXEBIS, design and initial commissioning results*, *AIP Conf. Proc.* **572** (2000) 59.

[29] E. Kugler, *The ISOLDE facility*, *Hyperfine Interact.* **129** (2000) 23.

[30] A. Kramida and Y. Ralchenko, *NIST Atomic Spectra Database*, NIST Standard Reference Database 78 (1999), DOI:10.18434/T4W30F.

[31] J. Angot et al., *Method for estimating charge breeder ECR ion source plasma parameters with short pulse 1+ injection*, *Plasma Sources Sci. Tech.* **30** (2021) 035018 [arXiv:2103.03546].

[32] R. Becker, O. Kester and T. Stoehlker, *Simulation of charge breeding for trapped ions*, *J. Phys. Conf. Ser.* **58** (2007) 443.

[33] V.P. Shevelko and H. Tawara, *Semiempirical formulae for multiple ionization of neutral atoms and positive ions by electron impact*, *J. Phys. B* **28** (1995) L589.

[34] M.F. Gu, *The flexible atomic code*, *Can. J. Phys.* **86** (2008) 675.

[35] L. Bowen, private communication, Lanzhou University (2024).

2025 JINST 20 C03053